# Fracture behavior of $Zr_{55}Cu_{30}Al_{10}Ni_5$ bulk metallic glass under quasi-static and dynamic compression

R.Q. Yang, J.T. Fan, S.X. Li, and Z.F. Zhang[a)]
*Shenyang National Laboratory for Materials Science, Institute of Metal Research, Chinese Academy of Sciences, Shenyang 110016, People's Republic of China*

Fracture behavior of $Zr_{55}Cu_{30}Al_{10}Ni_5$ bulk metallic glass was investigated under quasi-static compression at strain rate of $10^{-4}$/s using an Instron testing machine and dynamic split Hopkinson bar (SHPB) compression with strain rate of about 1900–4300/s. Pronounced strain softening, especially past the peak stress, was observed under SHPB tests and compared with the distinct flow serrations under quasi-static tests. Scanning electron microscope revealed that the angle between the loading axis and major shear plane is less than 45°, deviating from the maximum shear stress plane. Microscopically, unlike the ordinary veinlike pattern found in quasi-static compression, the elongated veinlike pattern was observed at the onset position of rapid shearing under dynamic test. A closely arrayed dendritelike structure dominated the dynamic fracture, consequently, and should be the major pattern representing the rapid shear band propagation. In addition, a transition state from veinlike to dendritelike pattern was observed at the final instantaneous fracture region in quasi-static tests. Evidence revealed the characteristic dimension of dynamic fracture surface complies with Taylor's meniscus instability criterion. The roles of free volume and adiabatic heating on the fracture strength and stress concentration on the fracture morphology are also discussed.

## I. INTRODUCTION

Since the early 1990s, new Zr-based multicomponent glass-forming alloys, such as Zr–Cu–Al–Ni[1] and Zr–Ti–Cu–Ni–Be,[2] with very high glass-forming ability (GFA) have been discovered. Because of their low critical cooling rate, sizable bulk metallic glasses (BMGs) have been fabricated with conventional casting methods. Zr-based BMGs exhibit superior engineering properties such as high fracture strength under ambient static pressure, high hardness, soft magnetism, and good corrosion resistance.[3,4] This class of BMGs can potentially be used in many commercial and industrial applications and even be used as kinetic penetrator.

However, during industrial use, many components may experience dynamic loading. It is particularly essential to quantify BMGs' dynamic constitutive behavior. Although the quasi-static mechanical properties and structural performance, as well as the deformation and fracture mechanisms of metallic glasses have been extensively studied,[5–15] there have been limited investigations on the dynamic properties of monolithic BMGs.

They indicate that BMGs have remarkably high fracture toughness comparable to that of structural steels[14–17] if a relatively low value of $\mu/B$ (ratio of the BMG's intrinsic elastic shear modulus $\mu$ to the bulk modulus $B$) is satisfied.[17] Localized shear bands usually dominate when they deform at room temperature (RT) under quasi-static,[10–12] Hopkinton pressure bar,[18–26] and shock wave[27,28] compression tests. Limited investigations have concentrated on the strain rate dependence of BMGs, as summarized in Table I. For $Zr_{41.2}Ti_{13.8}Cu_{12.5}Ni_{10}Be_{22.5}$ BMG, Bruck et al. reported that strength was insensitive to the strain rate,[18] consistent with other reports on the same alloy.[19,20] However, in $Pd_{40}Ni_{40}P_{20}$[21] and $Zr_{57}Ti_5Cu_{20}Ni_8Al_{10}$[22] BMGs, strain-rate softening at RT has been reported, which was also observed in Zr/Hf-based BMGs.[23,24] The latest report has shown greater negative strain-rate sensitivity exhibited by samples with smaller L/D ratios in $Zr_{41.2}Ti_{13.8}Cu_{12.5}Ni_{10}Be_{22.5}$ BMG.[26] In contrast, there is only one abnormal report on the strain-rate hardening behavior in $Nd_{60}Fe_{20}Co_{10}Al_{10}$ BMG.[25] This will be excluded from the following discussion since the reported strength was less than 1 GPa.

Besides the documented dynamic constitutive behavior, rapid failure surface characterizations of BMGs' are still lacking. The goal of this work was to examine the dynamic compressive fracture behavior of $Zr_{55}Cu_{30}Al_{10}Ni_5$

TABLE I. Dependence of fracture stress on strain rate in some BMGs.

| Group No. | Investigators | Composites | Static fracture stress (MPa) | Dynamic fracture stress (MPa) | Strain rate dependence at RT | $T_g/T_m = T_{rg}$ (K/K) |
|---|---|---|---|---|---|---|
| 1 | Bruck et al.[18] | $Zr_{41.2}TI_{13.8}Cu_{12.5}Ni_{10}Be_{22.5}$ (Vitreloy-1) | 1900 | $\approx 1900^{18}$ at $4.4 \times 10^3$/s | $\rightarrow$ | $623/932{-}0.67^{13}$ |
|  | Subhash et. al.[19] |  |  |  | $\rightarrow$ |  |
|  | Lu et. al.[20] |  |  |  | $\rightarrow$ |  |
| 2 | Hufnagel et. al.[22] | $Zr_{57}Ti_5Cu_{20}Ni_8Al_{10}$ | $\approx 1700$ | $\approx 1220$ at $4.4 \times 10^3$/s | $\downarrow 28\%^a$ | $676.7/1095.3 = 0.62^{13}$ |
|  | Li et. al.[23] |  | $\approx 1600$ | $\approx 1200$ at $2.8 \times 10^3$/s | $\downarrow 25\%^a$ |  |
|  | Mukai et. al.[21] | $Pd_{40}Ni_{40}P_{20}$ | $\approx 1750$ | $\approx 1580$ at $1.7 \times 10^3$/s | $\downarrow 10\%^a$ | $590/877.3 = 0.67^{13}$ |
|  | Li et. al.[23] | $Hf_{52.5}Ti_5Ni_{14.6}Cu_{17.9}Al_{10}$ | $\approx 2100$ | $\approx 1700$ at $3.1 \times 10^3$/s | $\downarrow 19\%^a$ | $770/1260 = 0.62^{24}$ |
|  | Gu et. al.[24] |  |  | $\approx 1550$ at $2 \times 10^3$/s | $\downarrow 26\%^a$ |  |
|  | Present results | $Zr_{55}Cu_{30}Al_{10}Ni_5$ | 1900 | 1060 at $3.4 \times 10^3$/s | $\downarrow 44\%^a$ | $680/1030 = 0.66$ |

Note: $T_g$, glass transition temperature; $T_m$, onset melting point; and glass-forming ability represented by reduced glass transition temperature $T_{rg}$.
a$\downarrow 28\%$ means the strength reduces 28% of the quasi-static value at the elevated strain rate; $\rightarrow$ indicates the strength is insensitive to the strain rate.

BMG using a split Hopkinson bar (SHPB) apparatus at RT. For comparison, quasi-static compressive tests were also carried out. The evolution of fracture surface features with increase in strain rate and their relation to fracture strength and plasticity were also investigated. The results shed light on the fracture mechanism of BMGs under high strain rate.

## II. EXPERIMENTAL PROCEDURE

Master alloy ingot with a nominal composition of $Zr_{55}Cu_{30}Al_{10}Ni_5$ (at.%) was prepared with a mixture of high-purity (5N) constituents and was cast into a copper mold in the highly pure argon atmosphere with a diameter of 3 mm using an arc-melting apparatus (NISSIN GIKEN type NEV-ACH3) after remelted for several times. Then the final ingot was analyzed by x-ray diffraction (XRD) using a Rigaku (Tokyo, Japan) diffractometer with Cu-radiation source. The results show only broad diffraction maxima without the peaks of crystalline phases, revealing the fully amorphous structure of the sample (Fig. 1).
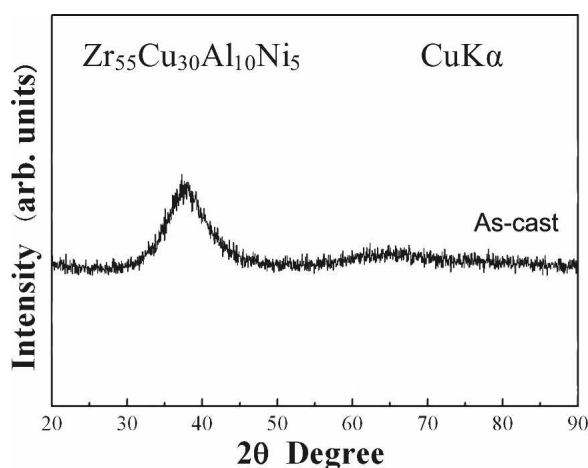


FIG. 1. XRD pattern taken from as-cast $Zr_{55}Cu_{30}Al_{10}Ni_5$ BMG, indicating a single glassy phase.

Quasi-static compressive tests were conducted on the BMG samples having dimensions of $\Phi$3 mm × 6 mm with a computer-controlled, servo-hydraulic INSTRON-8801 (Instron Corp., Norwood, MA) testing machine at a strain rate of $1 \times 10^{-4}$/s at RT. Moreover, a SHPB apparatus, reviewed elsewhere,[29] was used to determine the dynamic compressive stress–strain response. The basic setup of a SHPB apparatus consists of two elastic pressure bars, known as the input bar and the output bar. A specimen is placed between the two bars. The present strain rates were determined to be about 1900–4300/s for the specimens with the same diameter of 3 mm and in different length along the impact direction. The striker, input, output, and unloading bars with a diameter of 13 mm were made from high strength steel to ensure the fully elastic deformation of the bars during the compression.

Under dynamic compression, specimens were often crushed by the input bar. To preserve the fracture surface, an aged maraging steel stopper ring was fixed around the specimen. The stopper ring was 5%–15% shorter than the specimen was. It can stop the input bar quickly after the macroscopical fracture. Finally, all the deformation and fracture morphologies were observed using Quanta-600 scanning electron microscope (SEM).

### III. RESULTS

#### A. Mechanical properties

Figure 2 shows the typical compressive engineering stress–strain curves of the present BMG at high strain rate of 1900/s together with at the quasi-static strain rate ($1 \times 10^{-4}$/s) at RT for comparison. It can be seen that at quasi-static strain rate, the BMG specimen displays an initial elastic deformation and then begins to yield at about 1.9 GPa, followed by a plastic strain of about 2.5% prior to catastrophic fracture. As also can be seen, after quasi-static yielding, distinct serrated plastic flow begins, registered as repeating cycles of a sloping stress decrease followed by elastic reloading. It is much different from
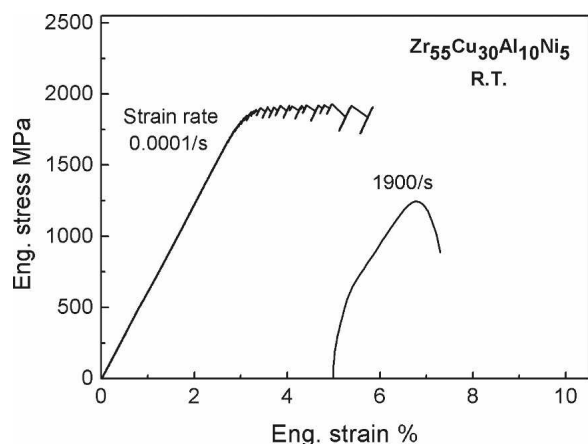
FIG. 2. Compressive stress–strain curves of $Zr_{55}Cu_{30}Al_{10}Ni_5$ at different strain rates.

the sudden vertical load drops (associated with the shear bands emission) in BMGs.[30] While the origin of this type of serrated flow is likely the shear band blunting and repropagating, there is presently no direct evidence.

In contrast to the quasi-static case, a pronounced decrease of the stress or strain softening, especially past the peak stress, is observed on the high-strain-rate stress–strain curves. At the strain rate of $1.9 \times 10^3/s$, the fracture strength drops to 1250 MPa, and at the strain rate of $3.4 \times 10^3/s$, only 1060 MPa remains. More than 40% strength was lost at this strain rate compared with the quasi-static strength. This is similar to that observed on Zr,[22,23] Pd,[21] and Hf-based[23,24] BMGs as illustrated in Table I, which contrasts sharply with the polycrystalline metals and alloy.[30,31] Another trend from Table I is that only one alloy so far, $Zr_{41.2}Ti_{13.8}Cu_{12.5}Ni_{10}Be_{22.5}$ (Vitreloy-1) containing beryllium, was found to have insensitive strain-rate dependence on the fracture strength. It remains constant from quasi-static strain rate to high strain rate of $4.4 \times 10^3 s^{-1}$.[18] The alloys in Table I are all BMGs and are all subjected to uniaxial compression. If we compare glass transition temperature $T_g$,[13] onset melting point $T_m$, and glass-forming ability (represented by reduced glass transition temperature $T_{rg}$), there is no obvious difference between Vitreloy-1 and other alloys. Therefore, it appears that the chemical composition may influence the nature of strain rate sensitivity of BMGs. The element beryllium may have special effects on the catastrophic failure resistance in Vitreloy-1 under dynamic circumstance.

It appears to be related to the local change in viscosity in shear bands under adiabatic conditions. There are two hypotheses as to why this happens. The first suggests that, during deformation, the viscosity within the shear bands decreases due to the formation of excess free volume.[6] The analysis by Bhowmick et al. showed the free volume was created during prior deformation. Formation of nanovoids was also postulated to appear afterward due

to the coalescence of the excess free volume. These nanovoids, in turn, lower the stress required for plastic deformation through shear bands.[32] The second contends that local adiabatic heating beyond the glass transition temperature, or even the melting temperature, occurs, decreasing the viscosity by several orders of magnitude.[7] Wright et al. predicted that the heating during the unloading segment of each serration under quasi-static loading is a few degrees Kelvin.[33] Bruck et al. observed that no adiabatic heating occurs before yielding in a Zr-based BMG.[18] The temperature rise during final fracture (from after the peak stress), however, may be much higher than that during the previous shear band operation. Evidence of ~500 K rise after fracture was observed,[18] along with a rise of over ~1000 K detected during impact fracture under nitrogen environment (to avoid oxidation).[34] The more recent experimental results of Lewandowski and Greer clearly demonstrate that temperature rise in the shear bands can be as high as a few thousand Kelvin over a few nanoseconds.[35] In the present, experiments features that appear to be resolidified droplets suggest that localized melting may have occurred during the final failure even under quasi-static tests [see Fig. 4(d)]. This hypothesis can be a proper explanation to the pronounced strain softening past the peak stress on the high-strain-rate stress–strain curve, due to the intense local adiabatic heating confined within shear bands.

Thus, we may conclude that, while the increase of free volume initiates the strain softening of BMGs, under adiabatic circumstances, the subsequent significant temperature rise greatly promotes the process, accelerating the localization of deformation and failure of the material.

In Fig. 3(a), secondary shear bands were found parallel to the major fracture plane, as indicated by the white arrows. However, no other shear bands parallel or inclined to the fracture plane can be easily distinguished on the dynamically deformed samples' side surface, as shown in Fig. 3(b). In addition, this side view of dynamically broken sample looks exactly like what was previous reported by Sunny et al. prior to the use of modified inserts, which implies stress concentration near the specimen–insert interface.[26] Under SHPB tests, the stress concentration and associated inhomogeneity of the stress state may also play an important role on the reduced fracture stress that was previously attributed in thermal softening.

## B. Evolution of veinlike structure

It has already been mentioned that both at quasi-static and high-strain-rate impact, the present BMG often fail along a single shear plane, indicating that one major shear band dominates the failure process. It is interesting to note that at a strain rate of $3.4 \times 10^3/s$, the catastrophic

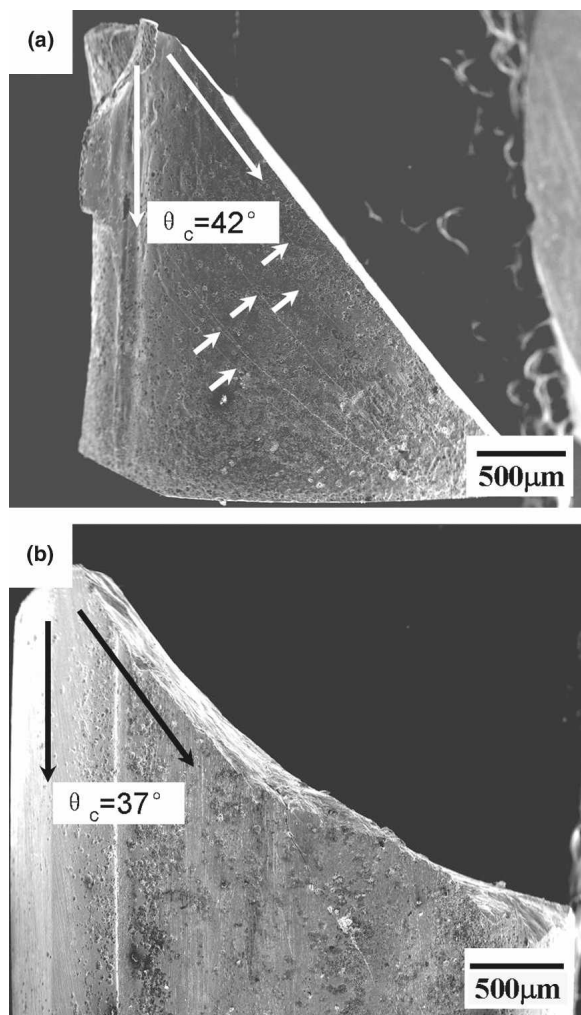FIG. 3. Appearance of the side surfaces of the specimens fractured at (a) quasi-static strain rate of $1 \times 10^{-4}$/s and (b) high strain rate of $3.4 \times 10^3$/s.

failure of the BMG occurred along a plane inclining about 37° with respect to the loading axis, as shown in Fig. 3(b), and the angle would change slightly at other high strain rates. While under quasi-static compression, the BMG failed along a shear plane of about 42°, as shown in Fig. 3(a). These angles all deviate from 45° maximum shear stress plane, demonstrating that yielding in the present BMGs follows the Mohr–Coulomb criterion, rather than the Tresca criterion.[8,10,12,36–38] This indicates that the normal stress on the shear plane always plays an important role in the shear fracture, no matter whether under quasi-static or under high strain rate compression. However, under SHPB tests, the stress concentration near the specimen–insert interface may not be left out of the account, as this will affect the fracture plane angle as well as the fracture stress.[26]

The inclination angle of the fracture plane is slightly dependent on the strain rate, and the macroscopic failure surface also alters with strain rate. The fracture surface of

quasi-statically compressed specimens is flat and smooth, as shown in Fig. 3(a). In contrast, the fracture surface tested at high strain rates is relatively rough. The microscopic aspects of the fracture surface still change with strain rates. The SEM observations show that the typical feature of the quasi-statically fractured surfaces is a veinlike structure, as shown in Figs. 4(a) and 4(b). This veinlike structure often spreads over the whole fracture surface and extends along a uniform direction (the propagation direction), as marked by the arrow in Fig. 4(b). The veinlike structure is attributed to lowered local viscosity within the main shear band induced by the high elastic energy release in instantaneous fracture.[39,40]

The typical morphologies of dynamically fractured surfaces are shown in Fig. 5. Unlike the ordinary veinlike structure observed under quasi-static circumstance, the individual veinlike pattern was elongated along the crack propagation direction at the sites of initial rapid shearing, as shown in Fig. 5(a). Another distinct morphology, a dendritelike/ridgelike structure, was also observed, as illustrated in Figs. 5(b)–5(d). They have very closely arrayed or refined "ridges." The mean distances between ridges in Figs. 5(c) and 5(d) along the indicated lines are about 1.9 and 0.9 μm, respectively. The closest spacing in the investigating area is about 0.6 μm, as illustrated by arrows in Fig. 5(d). This structure was seldom observed in the previous quasi-static tests.

## IV. DISCUSSION

As mentioned above, the fracture strength changes with the increase in strain rate. The fracture morphology also changes with it. Figure 4(a) demonstrates the typical fracture morphology when a crack propagates slowly. The individual plastic zone borders on each other like honeycomb. No obvious propagation direction can be detected from the pattern. Figure 4(b) shows an ordinary veinlike pattern when the material shearing off with a little bit higher velocity comparing with the former condition. At the time of final fracture under quasi-static compression, crack tips may suffer much rapid shearing rate. Figure 4(c) locates at the site that can serve as the region transiting from low to high strain rate deformation. It contains two patterns, veinlike and dendritelike. The latter is the common morphology observed on the dynamically fractured surface. With increase in strain rate, the dendritelike pattern dominates the fracture surface in SHPB compression test. Figure 6 sketchily illustrates the representative patterns of the veinlike pattern and the dendritelike pattern under quasi-static and dynamic compression, respectively. It should be pointed out that the dendritelike pattern does not cover the whole fracture surface. For the onset moment of rapid shearing, the elongated veinlike pattern can be observed [Fig. 5(a)], and afterward the dendritelike pattern covers most
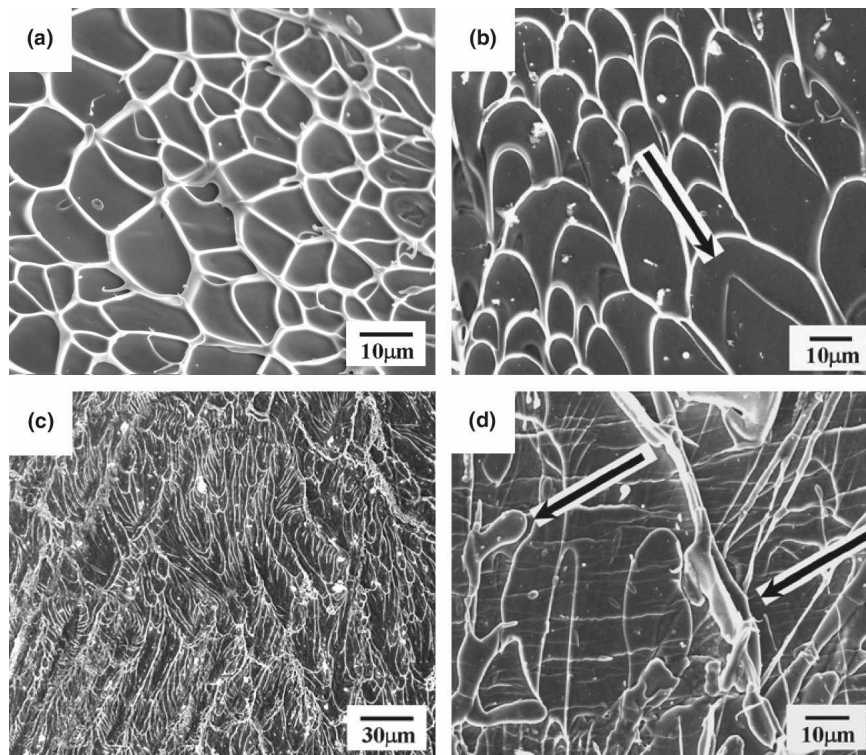
FIG. 4. SEM micrographs revealing the quasi-statically compressed fracture surface of $Zr_{55}Cu_{30}Al_{10}Ni_5$ BMG: (a) distinct directionless fracture pattern, (b) veinlike pattern with shearing direction indicated by the arrow, (c) transition from veinlike to dendritelike pattern, and (d) features that appear to be resolidified droplets, as indicated by arrows.
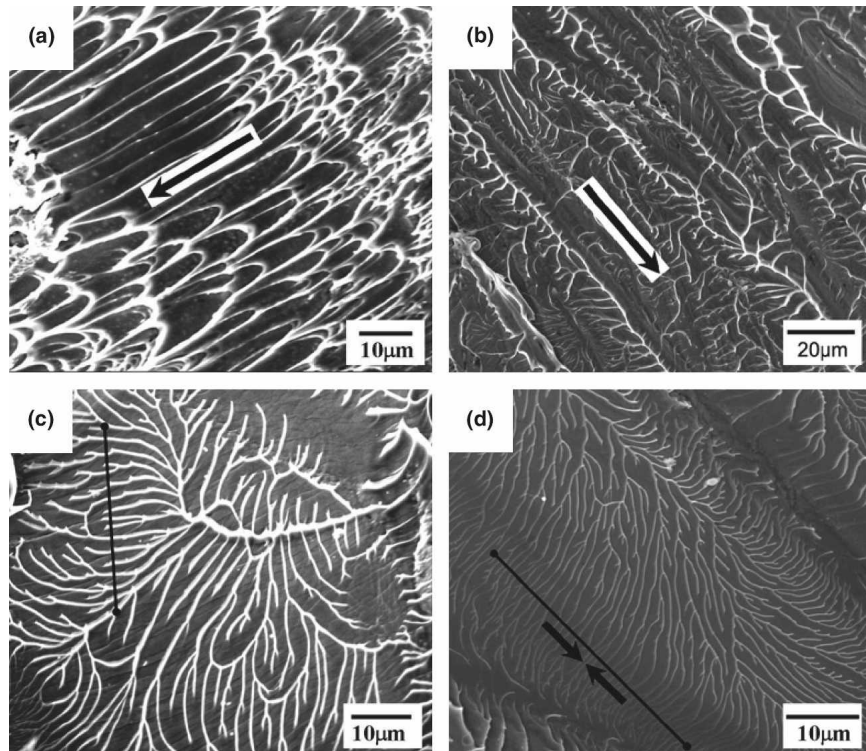


FIG. 5. SEM micrographs revealing the dynamic compression fracture surface of $Zr_{55}Cu_{30}Al_{10}Ni_5$ BMG: (a) elongated veinlike pattern, (b) dendritelike pattern that dominates the fracture surface, and (c, d) dendritelike patterns at different sites and at different magnifications.
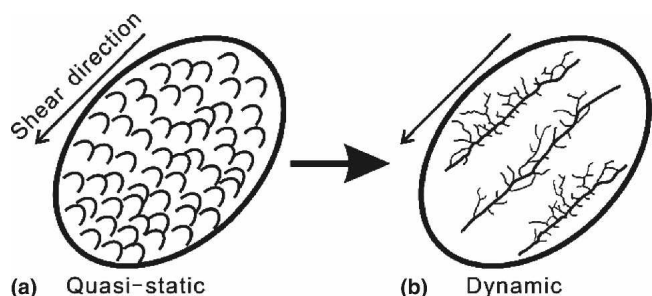
FIG. 6. Illustration of fracture morphology transition with increase in strain rates: (a) veinlike pattern under quasi-static compression and (b) dendritelike pattern under impact loading.

of the area. This dendritelike pattern was only commonly observed under high strain rate circumstance and should be the representative of shear band/cracks' rapid propagation.

For pure, simple fluids, including glassy metals, which behave in an ideally plastic manner, the dimension of their characteristic fracture surface features can be estimated by applying Taylor's meniscus instability criterion.[5] The spacing $\lambda_s$ between ridges on the fracture surface at the point of fast fracture can be estimated as follows

$$\lambda_s = 12\pi^2 A(n)\left(\frac{\chi}{\tau}\right) \quad . \tag{1}$$

Here, $\chi$ is the surface tension of the material. $A(n)$ is the coefficient of the nonlinearity exponent $n$. $\tau$ can be regarded as the shear yielding strength. For media with close to ideal plastic flow, $n$ will decrease to about 0.1 resulting in a small value of $A(n) = 2$. For the $Ni_{49}Fe_{29}P_{14}B_6Si_2$[41] glass strip rapidly failed in plane strain, they calculated $\lambda_s$ (the mean distance between ridges) to be 0.2 $\mu$m, which is very close to their experimental observation. If Eq. (1) is applied to the present BMG with the assumption that it has the same $\chi$ (~2000 ergs/cm$^2$) as $Ni_{49}Fe_{29}P_{14}B_6Si_2$ strip, $\lambda_s \approx 0.5$ $\mu$m can be obtained. The calculated value agrees well with the present mean spacing, especially with the closest ones.

The model of Eq. (1) has a precondition that treated the fracture medium as a nonlinear fluid.[5] Because of the high stain rate of SHPB impact, the small plastic zone ahead of the shear band/crack tip can be sufficiently heated because of the rapid propagation, leading to the fluidlike state of glassy metals. This idealization can be substantially close to the truth for the present high strain rate test. Therefore, the dendritelike structure should be the typical morphology, representing shear band/cracks' rapid propagation.

## V. CONCLUSIONS

The compressive fracture behavior of $Zr_{55}Cu_{30}Al_{10}Ni_5$ was characterized at quasi-static and high strain rate at RT. The following conclusions can be drawn.

Distinct serrated flow was observed on the stress–strain curves at quasi-static strain rate of $1 \times 10^{-4}$/s, in contrast with the pronounced strain softening past the peak stress observed on the high strain rate stress–strain curve. Under adiabatic circumstances, increase of free volume at the initial stage and the subsequent significant temperature rise were believed to accelerate the behavior of strain softening of BMGs.

The present BMG usually failed along a single shear plane in all tests. The plane inclines approximately 42° with respect to the loading axis at quasi-static strain rate and 37° at high strain rate of $3.4 \times 10^3$/s. The shear-off angle suggests that the yielding of $Zr_{55}Cu_{30}Al_{10}Ni_5$ obeys the Mohr–Coulomb criterion at all testing rates. Under SHPB tests, stress concentration near the specimen-insert interface may also affect the fracture plane angle.

A close examination of the fracture surface reveals that the veinlike structure evolves with strain rates. Under SHPB compression, the veinlike pattern changed into a dendritelike pattern, indicating a fluidlike state at the shear band/crack tips under the elevated strain rate.

## REFERENCES

1. T. Zhang, A. Inoue, and T. Masumoto: Amorphous Zr–Al–Tm (Tm = Co, Ni, Cu) alloys with significant supercooled liquid region of over 100 K. *Mater. Trans., JIM* **32,** 1005 (1991).
2. A. Peker and W.L. Johnson: A highly processable metallic glass $Zr_{41.2}Ti_{13.8}Cu_{12.5}Ni_{10}Be_{22.5}$. *Appl. Phys. Lett.* **63,** 2342 (1993).
3. A. Inoue, K. Ohtera, M. Kohinata, A-P. Tsai, and T. Masumoto: Glass transition behavior of Al- and Mg-based amorphous alloys. *J. Non-Cryst. Solids* **117,** 712 (1990).
4. W.L. Johnson: Bulk glass-forming metallic alloys: Science and technology. *MRS Bull.* **24**(10), 42 (1999).
5. A.S. Argon and A. Salama: The mechanism of fracture in glassy matrials capable of some inelastic deformation. *Mater. Sci. Eng.* **23,** 219 (1976).
6. F. Spaepen: A microscopic mechanism for steady state inhomogeneous flow in metallic glasses. *Acta Metall.* **25,** 407 (1977).
7. H.J. Leamy, T.T. Wang, and H.S. Chen: Plastic flow and fracture of metallic glass. *Metall. Mater. Trans.* **3,** 699 (1972).
8. P.E. Donovan: A yield criterion for $Pd_{40}Ni_{40}P_{20}$ metallic glass. *Acta Metall.* **37,** 445 (1989).

9. W.L. Johnson: Fundamental aspects of bulk metallic glass formation in multicomponent alloys. *Mater. Sci. Forum* **225,** 35 (1996).

10. P. Lowhaphandu, S.L. Montgomery, and J.J. Lewandowski: Effects of superimposed hydrostatic pressure on flow and fracture of Zr–Ti–Ni–Cu–Be bulk metallic glass. *Scripta Metall. Mater.* **41,** 19 (1999).

11. P. Lowhaphandu, L.A. Ludrosky, S.L. Montgomery, and J.J. Lewandowski: Deformation and fracture toughness of a bulk amorphous Zr–Ti–Ni–Cu–Be alloy. *Intermetallics* **8,** 487 (2000).

12. J.J. Lewandowski and P. Lowhaphandu: Pressure effects on flow and fracture of a bulk amorphous Zr–Ti–Ni–Cu–Be alloy. *Philos. Mag. A* **82,** 3427 (2002).

13. W.H. Wang, C. Dong, and C.H. Shek: Bulk metallic glasses. *Mater. Sci. Eng., R* **44,** 45 (2004).

14. C.J. Gilbert, R.O. Ritchie, and W.L. Johnson: Fracture toughness and fatigue-crack propagation in a Zr–Ti–Ni–Cu–Be bulk metallic glass. *Appl. Phys. Lett.* **71,** 476 (1997).

15. P. Lowhaphandu and J.J. Lewandowski: Fracture toughness and notched toughness of bulk amorphous alloy: Zr–Ti–Ni–Cu–Be. *Scripta Mater.* **38,** 1811 (1998).

16. N. Nagendra, U. Ramamurty, T.T. Goh, and Y. Li: Effect of crystallinity on the impact toughness of a La-based bulk metallic glass. *Acta Mater.* **48,** 2603 (2000).

17. J.J. Lewandowski, W.H. Wang, and A.L. Greer: Intrinsic plasticity or brittleness of metallic glasses. *Philos. Mag. Lett.* **85,** 77 (2005).

18. H.A. Bruck, A.J. Rosakis, and W.L. Johnson: The dynamic compressive behavior of beryllium bearing bulk metallic glasses. *J. Mater. Res.* **11,** 503 (1996).

19. G. Subhash, R.J. Dowding, and L.J. Kecskes: Characterization of uniaxial compressive response of bulk amorphous Zr–Ti–Cu–Ni–Be alloy. *Mater. Sci. Eng., A* **334,** 33 (2002).

20. J. Lu, G. Ravichandran, and W.L. Johnson: Deformation behavior of the $Zr_{41.2}Ti_{13.8}Cu_{12.5}Ni_{10}Be_{22.5}$ bulk metallic glass over a wide range of strain-rates and temperatures. *Acta Mater.* **51,** 3429 (2003).

21. T. Mukai, T.G. Nieh, Y. Kawamura, A. Inoue, and K. Higashi: Effect of strain rate on compressive behavior of a $Pd_{40}Ni_{40}P_{20}$ bulk metallic glass. *Intermetallics* **10,** 1071 (2002).

22. T.C. Hufnagel, T. Jiao, Y. Li, L.Q. Xing, and K.T. Ramesh: Deformation and failure of $Zr_{57}Ti_5Cu_{20}Ni_8Al_{10}$ bulk metallic glass under quasi-static and dynamic compression. *J. Mater. Res.* **17,** 1441 (2002).

23. H. Li, G. Subhash, X.L. Gao, L.J. Kecskes, and R.J. Dowding: Negative strain rate sensitivity and compositional dependence of fracture strength in Zr/Hf based bulk metallic glasses. *Scripta Mater.* **49,** 1087 (2003).

24. X. Gu, T. Jiao, L.J. Kecskes, R.H. Woodman, C. Fan, K.T. Ramesh, and T.C. Hufnagel: Crystallization and mechanical behavior of (Hf, Zr)–Ti–Cu–Ni–Al metallic glasses. *J. Non-Cryst. Solids* **317,** 112 (2003).

25. L.F. Liu, L.H. Dai, Y.L. Bai, B.C. Wei, and G.S. Yu: Strain rate-dependent compressive deformation behavior of Nd-based bulk metallic glass. *Intermetallics* **13,** 827 (2005).

26. G. Sunny, J.J. Lewandowski, and V. Prakash: Effects of annealing and specimen geometry on dynamic compression of a Zr-based bulk metallic glass. *J. Mater. Res.* **22,** 389 (2007).

27. S. Zhuang, J. Lu, and G. Ravichandran: Shock wave response of a zirconium-based bulk metallic glass and its composite. *Appl. Phys. Lett.* **80,** 4522 (2002).

28. F. Yuan, V. Prakash, and J.J. Lewandowski: Spall strength and Hugoniot elastic limit of a Zr-based BMG under planar shock compression. *J. Mater. Res.* **22,** 402 (2007).

29. P.S. Follansbee: The Hopkinson bar, in *Metals Handbook,* 9th ed., Mechanical Testing (American Society for Metals, Metals Park, OH, 1985), p. 198.

30. W.J. Wright, R.B. Schwarz, and W.D. Nix: Localized heating during serrated plastic flow in bulk metallic glasses. *Mater. Sci. Eng., A* **319,** 229 (2001).

31. P.S. Follansbee and U.F. Kocks: A constitutive description of the deformation of copper based on the use of the mechanical threshold stress as an internal state variable. *Acta Metall.* **36,** 81 (1988).

32. V. Schulze and O. Vöhringer: Influence of alloying elements on the strain rate and temperature dependence of the flow stress of steels. *Metall. Mater. Trans. A* **31,** 825 (2000).

33. R. Bhowmick, R. Raghavan, K. Chattopadhyay, and U. Ramamurty: Plastic flow softening in a bulk metallic glass. *Acta Mater.* **54,** 4221 (2006).

34. C.J. Gilbert, J.W. Ager III, V. Schroeder, and R.O. Ritchiea: Light emission during fracture of a Zr–Ti–Ni–Cu–Be bulk metallic glass. *Appl. Phys. Lett.* **74,** 3809 (1999).

35. J.J. Lewandowski and A.L. Greer: Temperature rise at shear bands in metallic Glasses. *Nat. Mater.* **5,** 15 (2006).

36. Z.F. Zhang, J. Eckert, and L. Schultz: Difference in compressive and tensile fracture mechanisms of $Zr_{59}Cu_{20}Al_{10}Ni_8Ti_3$ bulk metallic glass. *Acta Mater.* **51,** 1167 (2003).

37. Z.F. Zhang, G. He, J. Eckert, and L. Schultz: Fracture mechanisms in bulk metallic glassy materials. *Phys. Rev. Lett.* **91,** 045505 (2003).

38. Z.F. Zhang and J. Eckert: Unified tensile fracture criterion. *Phys. Rev. Lett.* **94,** 094301 (2005).

39. C.A. Pampillo: Flow and fracture in amorphous alloys. *J. Mater. Sci.* **10,** 1194 (1975).

40. V.Z. Bengus, E.D. Tabachnikova, J. Miškuf, K. Csach, V. Ocelik, W.L. Johnson, V.V. Molokanov: New features of the low temperature ductile shear failure observed in bulk amorphous alloys. *J. Mater. Sci.* **35,** 4449 (2000).

41. L.A. Davis: Plastic instability in a metallic glass. *Scripta Metall.* **9,** 339 (1975).